New Journal of Physics
The open access journal at the forefront of physics

Deutsche Physikalische Gesellschaft DPG
IOP Institute of Physics

Published in partnership with: Deutsche Physikalische Gesellschaft and the Institute of Physics

OPEN ACCESS

RECEIVED
20 November 2014

REVISED
31 December 2014

ACCEPTED FOR PUBLICATION
7 January 2015

PUBLISHED
10 February 2015

PAPER

Localized versus itinerant states created by multiple oxygen vacancies in $SrTiO_3$

Harald O Jeschke, Juan Shen and Roser Valentí

Institut für Theoretische Physik, Goethe-Universität Frankfurt am Main, D-60438 Frankfurt am Main, Germany

E-mail: jeschke@itp.uni-frankfurt.de

Keywords: perovskite oxides, oxygen vacancies, density functional theory, electronic structure

Abstract

Oxygen vacancies in strontium titanate surfaces ($SrTiO_3$) have been linked to the presence of a two-dimensional electron gas with unique behavior. We perform a detailed density functional theory study of the lattice and electronic structure of $SrTiO_3$ slabs with multiple oxygen vacancies, with a main focus on two vacancies near a titanium dioxide terminated $SrTiO_3$ surface. We conclude based on total energies that the two vacancies preferably inhabit the first two layers, i.e. they cluster vertically, while in the direction parallel to the surface, the vacancies show a weak tendency towards equal spacing. Analysis of the nonmagnetic electronic structure indicates that oxygen defects in the surface TiO_2 layer lead to population of Ti t_{2g} states and thus itinerancy of the electrons donated by the oxygen vacancy. In contrast, electrons from subsurface oxygen vacancies populate Ti e_g states and remain localized on the two Ti ions neighboring the vacancy. We find that both the formation of a bound oxygen-vacancy state composed of hybridized Ti $3e_g$ and 4p states neighboring the oxygen vacancy as well as the elastic deformation after extracting oxygen contribute to the stabilization of the in-gap state.

1. Introduction

The discovery of a two-dimensional (2D) electron gas at the interface between $SrTiO_3$ (STO) and $LaAlO_3$ (LAO) in an LAO/STO heterostructure by Ohtomo and Hwang [1] initiated intense research efforts [2, 3] on these materials and unexpected phases at the interface like superconductivity [4] and ferromagnetism [5] were reported. However, there has been some controversy on the mechanisms leading to the conducting interface, with proposals ranging from electronic reconstruction as a way to avoid a polar catastrophe [6] to various mechanisms based on extrinsic defects like oxygen vacancies [7, 8] and site disorder [9, 10]. More recently, a metallic state has also been discovered at the surfaces of freshly cleaved $SrTiO_3$ [11, 12] and $KTaO_3$ [13, 14]. In the case of pure $SrTiO_3$ surfaces, the metallic state and the photoemission spectra can be well explained with oxygen vacancies [11, 15, 16]. Besides the spectral weight at the Fermi level, the presence of a peak at about 1.3 eV below the Fermi level was also reported [11]. Aiura *et al* [17] observed in photoemission experiments for lightly electron-doped $SrTiO_3$ under different oxygen pressure conditions, that the peak at 1.3 eV appears to depend on the oxygen defect density. As pristine $SrTiO_3$ is a semiconductor with a large band gap of $E_g = 3.2$ eV, creating a number of Ti t_{2g} carriers and assuming a rigid band shift should lead to a photoemission spectrum with a wide gap below the states near the Fermi level. However, several experiments [11, 12, 17–20] show that the $E = -1.3$ eV feature is robust and reproducible but sensitive to oxygen pressure. Understanding the nature and orbital character of the $E = -1.3$ eV feature as well as the interplay between localized and itinerant states created by the presence of oxygen vacancies will be the main focus of our study. In fact, the role of oxygen vacancies is presently being intensively discussed in a wider context of materials. For instance, oxygen vacancies have been proposed to be responsible for the suppression of the metal–insulator transition in VO_2 [21], as well as for the electron beam-induced growth of iron nanowires on TiO_2 [22], to mention a few. Therefore, getting a deeper microscopic

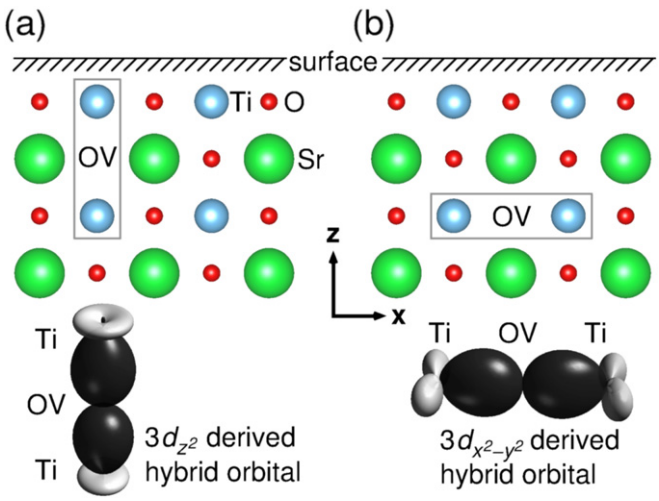

Figure 1. Schematic view of two inequivalent subsurface oxygen vacancy positions together with a sketch of the symmetry of the resulting hybrid orbitals on the Ti sites next to the oxygen vacancy.

understanding of the role of oxygen vacancies in transition metal oxides can further elucidate the mechanisms behind the above observed phenomena.

There have been a number of previous theoretical efforts dealing with oxygen vacancies in $SrTiO_3$. Cuong *et al* [23], using LDA+U calculations, found that oxygen vacancies in bulk $SrTiO_3$ tend to cluster in a linear fashion. Hou and Terakura [24] performed GGA+U calculations of single and double oxygen vacancies in bulk $SrTiO_3$. Several calculations based on hybrid functionals [25, 26] or LDA+U [27] have found an oxygen defect related in-gap state for $SrTiO_3$. Lin and Demkov [28] used a three-orbital Hubbard model to study the effect of electronic correlation on an oxygen vacancy in $SrTiO_3$. Pavlenko *et al* [29] analyzed the orbital reconstruction at $SrTiO_3/LaAlO_3$ interfaces due to oxygen vacancies within GGA+U. We will extend this existing work by (i) focusing on $SrTiO_3$ surfaces and by (ii) using large supercells that allow us to investigate two and three oxygen vacancies at realistic defect densities.

In our study we show that (i) multiple subsurface oxygen defects are energetically less favorable than configurations with at least one defect in the TiO_2 surface layer. (ii) Vertically, defects show a clear tendency to cluster; defect configurations with two oxygen defects in the first two layers (surface TiO_2 and first subsurface SrO layer) are clearly preferred over configurations with one or two layers of vertical distance between the two vacancies. In contrast, in the direction parallel to the surface, we find a tendency of vacancies to distribute uniformly. (iii) Moreover, while the isolated surface oxygen vacancy creates itinerant Ti t_{2g} electrons, the subsurface vacancy creates two localized states of Ti e_g character in the two adjacent Ti ions. The localized states have $3d_{z^2}$ character with some $4p_z$ weight for oxygen vacancies in a subsurface SrO layer, and $3d_{x^2-y^2}$ character with some $4p_x/p_y$ weight for vacancies in a subsurface TiO_2 layer (see figure 1). Finally, we also show that (iv) the precise condition for an in-gap state produced from surface vacancies is the formation of a $TiO_3(\text{vacancy})_2$ cluster.

2. Method

In order to investigate the role of oxygen vacancies in $SrTiO_3$, we performed density functional theory calculations for a number of $SrTiO_3$ slabs with various configurations of oxygen vacancies and analyzed the origin of the states appearing near the Fermi level. We have considered stoichiometric $SrTiO_3$ slabs with (001) surfaces, as discussed in [15]. We consider neutral oxygen vacancies. Based on our previous experience, we use $3 \times 3 \times 4$ supercells with TiO_2 termination; we have also performed calculations for slabs with vacancies in SrO terminated surfaces but in the present work we focus on the TiO_2 termination which is more relevant experimentally. We use the energetically most favorable structures with a single vacancy in the TiO_2 surface layer as a starting point for structures with a second or even a third oxygen defect. We relax these structure candidates using the Vienna *ab initio* simulation package [30, 31] with the projector augmented wave basis [32]. As it has been found that relaxations with the generalized gradient approximation (GGA) [34] tend to make the octahedral environment of transition metal ions too homogeneous [33] we use a GGA+U functional [35] with

literature values for $SrTiO_3$ [36] of $U = 5$ eV and $J = 0.64$ eV. We analyze the electronic structure and total energy of the predicted slab geometries using an all electron full potential local orbital [37] basis.

3. Results

In figure 2, we show examples of $SrTiO_3$ supercells with two oxygen vacancies. They correspond to the energetically most favorable configurations with the first vacancy in the TiO_2 surface layer (layer 1) and the second vacancy in (a) the surface layer (layer 1), (b) the first subsurface SrO layer (layer 2), (c) the first subsurface TiO_2 layer (layer 3) or (d) the second subsurface SrO layer (layer 4). An overview of the energetics is shown in figure 3. Energies are given with respect to the energy E_0 of the configuration drawn in figure 2(b) which turned out to be the optimum. We find a clear trend: defect configurations with one vacancy on the surface (layer 1) and the second one in the first subsurface layer (layer 2) are energetically more favorable than configurations where the two oxygen vacancies are separated by one or two pristine layers. This means that there is a clear tendency of oxygen vacancies to cluster vertically near the surface of $SrTiO_3$. In the direction parallel to the surface, however, the outcome of our simulations is more complex. While configurations with both defects in the surface TiO_2 layer (circles in figure 3) show a weak tendency to cluster, the energetically most favorable corresponds to distributing one defect in the first (TiO_2) and one defect in the second (SrO) layer (triangle at $E = E_0$ in figure 3) with a maximal distance between the two vacancies within our simulation cell. This result suggests a tendency to uniform distribution of defects parallel to the surface. Turning to the defects separated by a pristine SrO layer from the surface oxygen defect (diamonds in figure 3), we observe a weak preference of defects to lower vacancy–vacancy separation, i.e. to cluster with the SrO spacer layer between the two defects. Note that structures with both vacancies below the TiO_2 surface are 1.4 eV and more higher in energy than the optimum and therefore do not appear in figure 3.

We now proceed with an analysis of the electronic structure of the two oxygen vacancy configurations. Figure 4 shows the density of states for all structures discussed before. Gray shading indicates electronic states which are populated with electrons donated by the oxygen vacancy. All investigated structures have Ti t_{2g} weight near the Fermi level. A detailed analysis of this weight shows that a large number of Ti ions in the supercell contribute to it and the corresponding bands are dispersive, indicating that these electrons are itinerant. We have shown in [15] that this is a result of structural relaxation; if all ions are kept in the ideal perovskite position upon creation of an oxygen vacancy, only Ti t_{2g} orbitals next to the vacancy are occupied, and an unphysical localized t_{2g} electron density is created. As in the previous study, the itinerancy of electrons is limited to a thin layer near the oxygen vacancies; in this sense, the on-site energies of the Ti atoms affected by the oxygen defect can be considered as a shallow trap as discussed in [38]. As a second important feature, all structures in figure 4(b) and all except the first one in figure 4(a) also show sharp in-gap states; these are states typically created by subsurface oxygen defects and localized on the two Ti ions adjacent to the defect. These states have Ti e_g character with small admixture of 4p states, and they clearly fall into two categories: Ti d_{z^2} states created by vacancies in a SrO layer, and Ti $d_{x^2-y^2}$ states produced by vacancies in subsurface TiO_2 layers. This orbital occupancy is due to the fact that in the case of an oxygen defect in a SrO layer, the Ti ions neighboring the defect are above and below the defect where the vertical axis corresponds to the z-axis in the orbital projection (see figure 1(a)). In the case of a subsurface defect in a TiO_2 layer, the two neighboring Ti ions sit at half a lattice spacing either along the x or y direction with respect to the vacancy (see figure 1(b)). Figure 5(a) and (b) illustrate the orbital distribution of the defect configuration shown in figure 2(b) where one vacancy is on the TiO_2 surface (layer 1) and the second vacancy is on the subsurface SrO layer (layer 2). Figure 5 (c) and (d) display the orbital distribution for a representative example of one vacancy on the TiO_2 surface (layer 1) and the second one on the TiO_2 subsurface (layer 3), as in figure 2(c).

In-gap states are also present when oxygen vacancies cluster at the surface TiO_2 layer (cases 3 and 4 in figure 4). Our calculations show that the precise condition for such in-gap states produced from surface vacancies is the formation of a $TiO_3(\text{vacancy})_2$ cluster. In fact, the energetically most favorable configuration with two vacancies in the surface TiO_2 layer (see figure 2(a)) is of this type. On the other hand, well separated oxygen vacancies in the surface TiO_2 layer which form $TiO_4(\text{vacancy})$ clusters only (cases 1 and 2 in figure 4) lead to an itinerant 2D electron gas of Ti t_{2g} electrons but no in-gap states.

In order to further test the distribution of oxygen-vacancy-induced extra charge, we also calculated the electronic properties of $3 \times 3 \times 4$ $SrTiO_3$ slabs with three oxygen vacancy configurations as shown in figure 6. In all three cases in-gap states appear below the Fermi level since some oxygen vacancies are either below the TiO_2 surface layer or they are clustered around a Ti on the surface. Comparison of the two-vacancy with the three-vacancy cases shows that the in-gap weight is proportional to the oxygen vacancy density. This observation is in qualitative agreement with experiment [17] but it should be investigated further. We found that two oxygen vacancies produce in-gap states with binding energies betweeen −0.4 and −0.8 eV which is significantly smaller

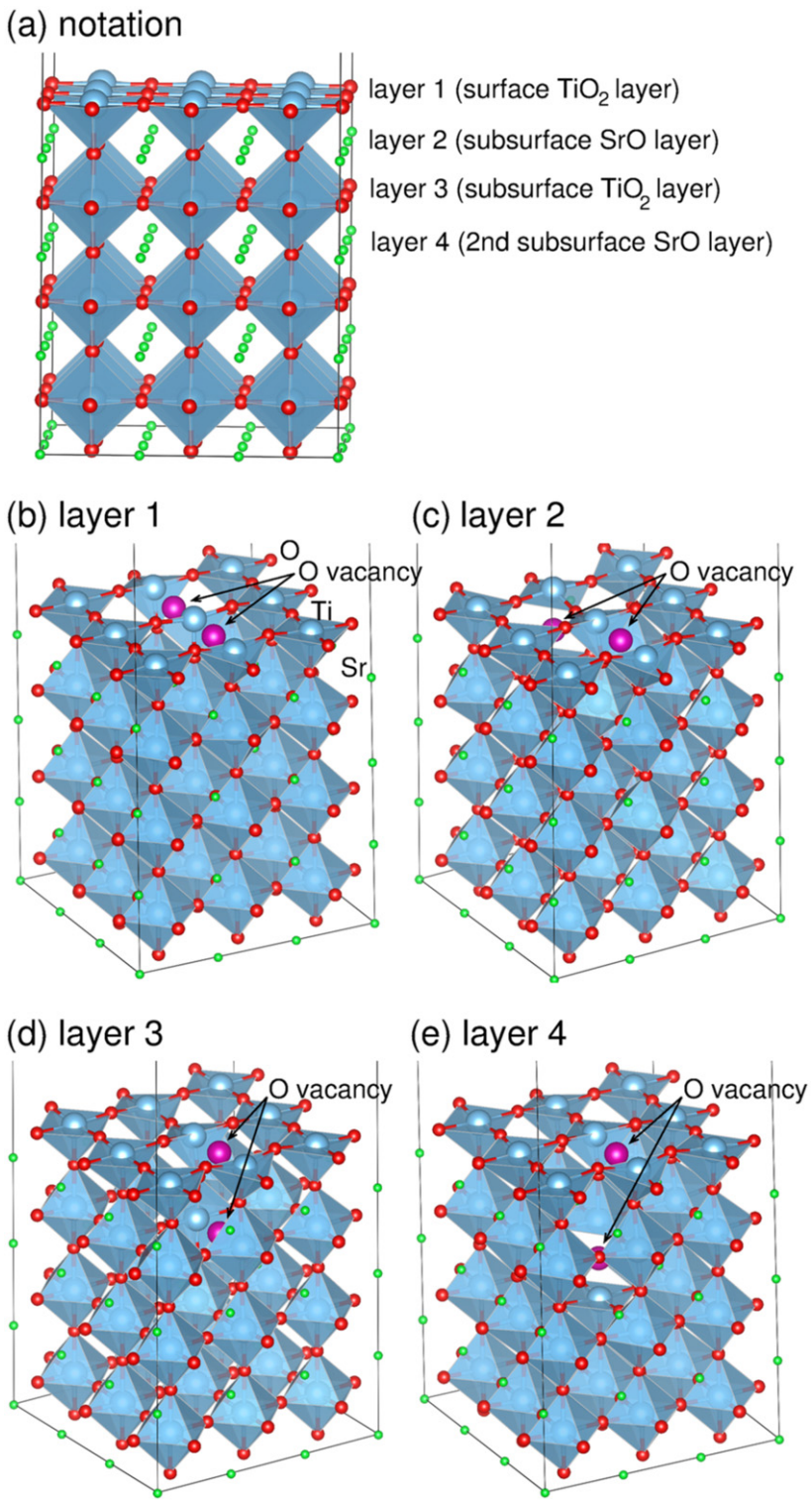

Figure 2. Examples of $SrTiO_3$ slab structures. $3 \times 3 \times 4$ perovskite units have been considered in the calculation and in (a) the notation used through the text is given. There are two oxygen vacancies: one is always in the surface TiO_2 layer (layer 1). Examples for the energetically most favorable positioning of the second oxygen vacancy in the surface layer (layer 1) are shown in (b), in the subsurface SrO layer (layer 2) in (c), in the first subsurface TiO_2 layer (layer 3) in (d) and in the second subsurface SrO layer (layer 4) in (e).

than the position of the peak at $E = -1.3$ eV observed experimentally. However, the three vacancies already lead to in-gap states with binding energies between −0.3 and −1.1 eV (see figure 7). This indicates that by including more vacancies in the calculation, we are approaching the position of the in-gap state observed in experiment. We have also tested the dependence of the in-gap peak position on the interaction parameter U of the GGA+U functional. We find that as expected larger U values lead to higher binding energies of the in-gap state. However,

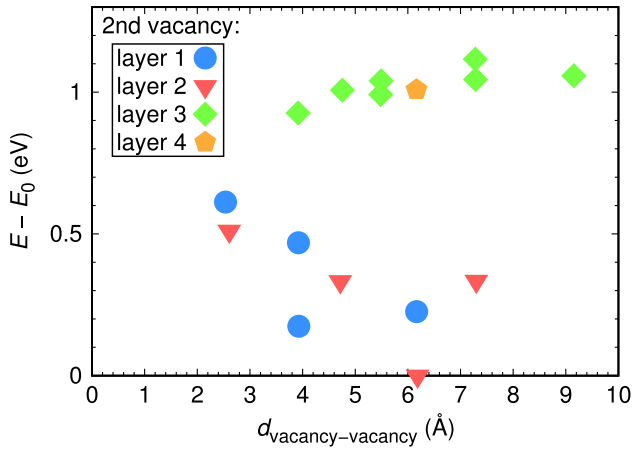

Figure 3. Total energies of $SrTiO_3$ slabs with two oxygen vacancies calculated within GGA+U. The first vacancy is always in the surface TiO_2 layer (layer 1). Energies are given as function of distance to the second vacancy which can be in the surface TiO_2 layer (layer 1) (circles), in the subsurface SrO layer (layer 2) (triangles), in the first subsurface TiO_2 layer (layer 3) (diamonds) or in the second subsurface SrO layer (layer 4) (pentagon).

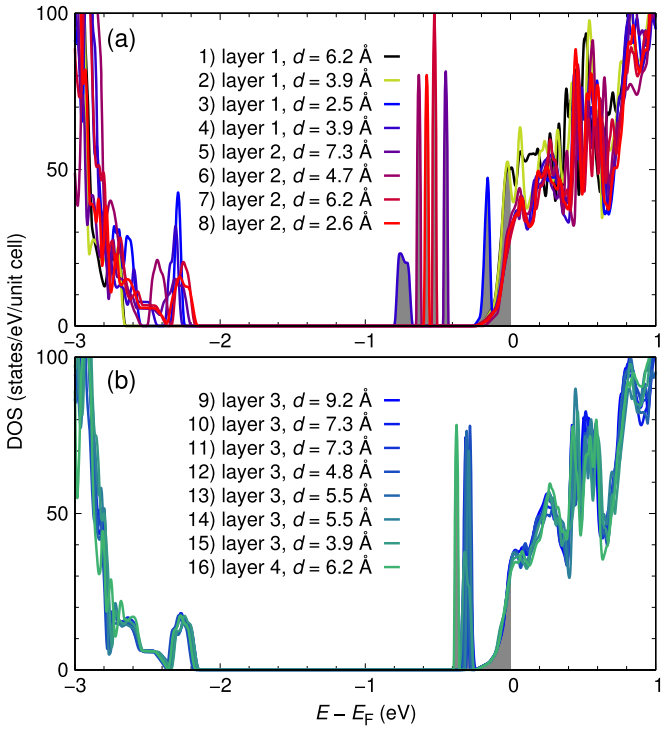

Figure 4. Densities of states for two oxygen vacancies in $3 \times 3 \times 4$ $SrTiO_3$ slabs calculated within GGA+U. The first vacancy is always in the surface TiO_2 layer. (a) Second vacancy in surface TiO_2 layer or in first subsurface SrO layer. All but the first two structures lead to an in-gap DOS peak. In the structure corresponding to DOS number 4, the two oxygen vacancies have a Ti in the middle, in contrast to DOS number 2. (b) Second vacancy in first surface TiO_2 layer or in second subsurface SrO layer. Number 4 is the DOS for the structure in figure 2(a), number 8 corresponds to figure 2(b), number 15 to figure 2(c) and number 16 to figure 2(d).

considering that GGA+U is only an approximate treatment of strong electronic correlations, we did not adjust the interaction parameters to shift the in-gap states to the experimentally observed position.

4. Discussion

Analysis of the previous LDA+U results allows us to draw some important conclusions regarding the role of oxygen vacancies in $SrTiO_3$. (1) If oxygen vacancies are only on the surface and well separated from each other, the two electrons per vacancy contribute *only* to the conduction band and no localized in-gap states are formed independently of the *U* value considered in the LDA+U calculations. Only when oxygen vacancies cluster on the

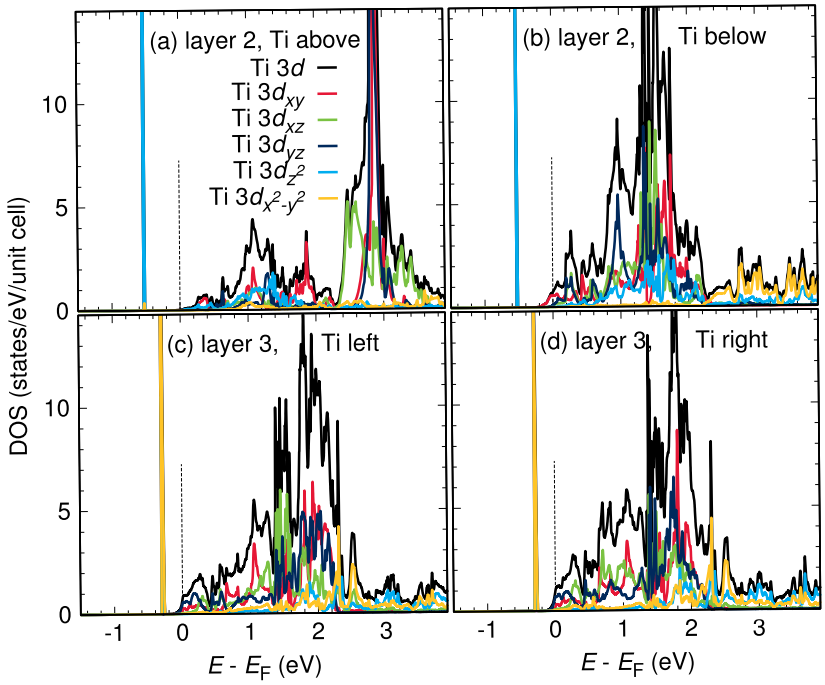

Figure 5. Partial densities of states for Ti ions neighboring oxygen vacancies. (a) and (b) Ti ions sitting above and below a vacancy in the first subsurface SrO layer. (c) and (d) Ti ions sitting right and left of a vacancy in the first subsurface TiO_2 layer.

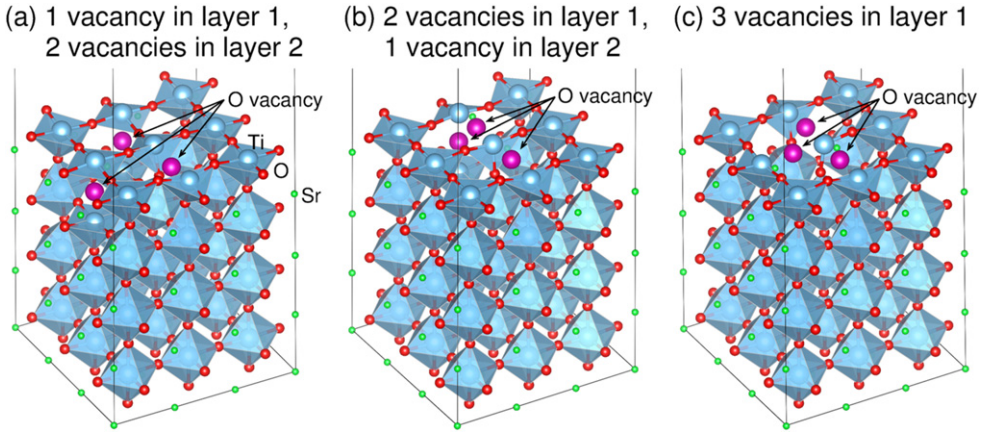

Figure 6. Three examples of three oxygen vacancy configurations in $3 \times 3 \times 4$ $SrTiO_3$ slabs.

surface, assuming $TiO_3(\text{vacancy})_2$ configurations, or are positioned in subsurface layers do we observe the formation of in-gap states coming from the hybridized $3e_g$ with 4p states from the Ti neighboring the vacancy. This is in contrast to a recent study by Lin *et al* [28] where it was suggested that the oxygen-vacancy-induced in-gap state traps at most one electron from the oxygen vacancy while the second electron contributes to the conduction. (2) The energy ordering of the different vacancies configurations with presence of in-gap states can be attributed to two effects: (i) the gain in energy due to the formation of a bound oxygen-vacancy state (in-gap state) composed of the hybridized Ti e_g and 4p states neighboring the vacancy as well as (ii) the gain in elastic energy due to the lattice deformation after extracting oxygen. In fact, calculations of total energies of relaxed versus unrelaxed slab structures point to a significant contribution of the second effect that should be considered together with the formation of the bound state. Moreover, the lattice deformation is important in the formation of an itinerant 2D electron gas due to surface oxygen vacancies. (3) The weight of the in-gap state scales with the oxygen vacancy concentration in agreement with photoemission experiments. (4) The formation energy of an oxygen vacancy in $SrTiO_3$ is about 7.7 eV for a single vacancy and 4.8 eV per vacancy for two and three vacancies. From our present calculations we can only speculate about possible formation mechanisms of such vacancies. Certainly the exposure to energetic photons in photoemission experiments is a possible cause. (5) The tendency

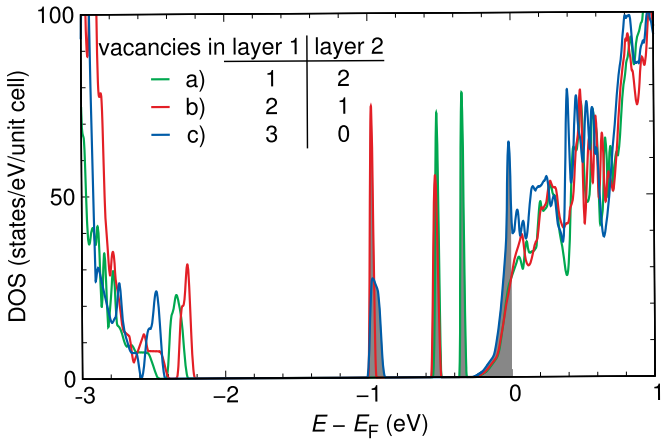

Figure 7. Densities of states for three examples of three oxygen vacancy configurations in 3 × 3 × 4 $SrTiO_3$ slabs calculated within GGA+U.

for vacancy clustering in the vertical direction, but not in the plane of the surface could be understood in terms of an effective vacancy–vacancy attraction by strain in the vertical direction, i.e. one vacancy takes advantage of the deformation induced by the other vacancy, similar to what happens in a bipolaron. This strain-mediated attraction competes with the Coulombic repulsion of the net charge of the vacancies. At short distances the former wins due to the generation of a deep trap that localizes the carriers (in-gap states) and thereby neutralizes the vacancies. We leave the study of this interplay as a function of the distance between vacancies for future work.

Finally, based on the present study of multiple oxygen vacancies near the $SrTiO_3$ surface, it will now be very interesting to extend such an investigation to multiple oxygen vacancies near the interfaces of oxide heterostructures such as $LaAlO_3/SrTiO_3$ where the polar character of the interface has been shown to strongly influence the behavior of oxygen vacancies [38, 39].

In summary, by considering different configurations of oxygen vacancies in $SrTiO_3$ and subsequent analysis of the energetics and electronic properties via extensive DFT calculations we can explain the origin of observed in-gap states as well as conduction electrons in photoemission experiments on $SrTiO_3$ surfaces and provide predictions for the behavior of a finite concentration of oxygen vacancies in $SrTiO_3$.

Acknowledgments

We thank K Muthukumar for running some test calculations at the initial stages of this work. We thank Ralph Claessen, Michael Sing, Andres Santander-Syro, Marc Gabay, Marcelo Rozenberg and Thilo Kopp for useful discussions and gratefully acknowledge financial support by the Deutsche Forschungsgemeinschaft (DFG) through grant FOR 1346. The generous allotment of computer time by CSC-Frankfurt and LOEWE-CSC is also gratefully acknowledged.

References

[1] Ohtomo A and Hwang H Y 2004 A high-mobility electron gas at the $LaAlO_3/SrTiO_3$ heterointerface *Nature* **427** 423
[2] Mannhart J, Blank D H A, Hwang H Y, Millis A J and Triscone J-M 2008 Two-dimensional electron gases at oxide interfaces *MRS Bull.* **33** 1027
[3] Huijben M, Brinkman A, Koster G, Rijnders G, Hilgenkamp H and Blank D H A 2009 Structure-property relation of $SrTiO_3/LaAlO_3$ interfaces *Adv. Mater.* **21** 1665
[4] Reyren N *et al* 2007 Superconducting interfaces between insulating oxides *Science* **317** 1196
[5] Brinkmann A, Huijben M, van Zalk M, Huijben J, Zeitler U, Maan J C, van der Wiel W G, Rijnders G, Blank D H A and Hilgenkamp H 2007 Magnetic effects at the interface between non-magnetic oxides *Nat. Mater.* **6** 493
[6] Okamoto S and Millis A J 2004 Electronic reconstruction at an interface between a Mott insulator and a band insulator *Nature* **428** 630
[7] Siemons W, Koster G, Yamamoto H, Harrison W A, Lucovsky G, Geballe T H, Blank D H A and Beasley M R 2007 Origin of charge density at $LaAlO_3$ on $SrTiO_3$ heterointerfaces: possibility of intrinsic doping *Phys. Rev. Lett.* **98** 196802
[8] Herranz G *et al* 2007 High mobility in $LaAlO_3/SrTiO_3$ heterostructures: origin, dimensionality, and perspectives *Phys. Rev. Lett.* **98** 216803
[9] Nakagawa N, Hwang H Y and Muller D A 2006 Why some interfaces cannot be sharp *Nat. Mater.* **5** 204
[10] Yu L and Zunger A 2014 A polarity-induced defect mechanism for conductivity and magnetism at polarnonpolar oxide interfaces *Nat. Commun.* **5** 5118
[11] Santander-Syro A F *et al* 2011 Two-dimensional electron gas with universal subbands at the surface of $SrTiO_3$ *Nature* **469** 189

[12] Meevasana W, King P D C, He R H, Mo S-K, Hashimoto M, Tamai A, Songsiriritthigul P, Baumberger F and Shen Z-X 2011 Creation and control of a two-dimensional electron liquid at the bare $SrTiO_3$ surface *Nat. Mater.* **10** 114
[13] King P D C *et al* 2012 Subband structure of a two-dimensional electron gas formed at the polar surface of the strong spin–orbit perovskite $KTaO_3$ *Phys. Rev. Lett.* **108** 117602
[14] Santander-Syro A F *et al* 2012 Orbital symmetry reconstruction and strong mass renormalization in the two-dimensional electron gas at the surface of $KTaO_3$ *Phys. Rev.* B **86** 121107 (R)
[15] Shen J, Lee H, Valentí R and Jeschke H O 2012 *Ab initio* study of the two-dimensional metallic state at the surface of $SrTiO_3$: importance of oxygen vacancies *Phys. Rev.* B **86** 195119
[16] Wang Z *et al* 2014 Anisotropic two-dimensional electron gas at $SrTiO_3$(110) *Proc. Natl Acad. Sci. USA* **111** 3933
[17] Aiura Y, Hase I, Bando H, Yasue T, Saitoh T and Dessau D S 2002 Photoemission study of the metallic state of lightly electron-doped $SrTiO_3$ *Surf. Sci.* **515** 61
[18] Courths R 1980 Ultraviolet photoelectron spectroscopy (UPS) and LEED studies of $BaTiO_3$ (001) and $SrTiO_3$ (100) surfaces *Phys. Status Solidi* B **100** 135
[19] Kim Y S, Kim J, Moon S J, Choi W S, Chang Y J, Yoon J-G, Yu J, Chung J-S and Noh T W 2009 Localized electronic states induced by defects and possible origin of ferroelectricity in strontium titanate thin films *Appl. Phys. Lett.* **94** 202906
[20] Hatch R C, Fredrickson K D, Choi M, Lin C, Seo H, Posadas A B and Demkov A A 2013 Surface electronic structure for various surface preparations of Nb-doped $SrTiO_3$ (001) *J. Appl. Phys.* **114** 103710
[21] Jeong J, Aetukuri N, Graf T, Schladt T D, Samant M G and Parkin S T P 2013 Suppression of metal–insulator transition in VO_2 by electric field-induced oxygen vacancy formation *Science* **339** 1402
[22] Vollnhals F, Woolcot T, Walz M-M, Seiler S, Steinrück H-P, Thornton G and Marbach H 2013 Electron beam-induced writing of nanoscale iron wires on a functional metal oxide *J. Phys. Chem.* C **117** 17674
[23] Cuong D D, Lee B, Choi K M, Ahn H-S, Han S and Lee J 2007 Oxygen vacancy clustering and electron localization in oxygen-deficient $SrTiO_3$: LDA+U study *Phys. Rev. Lett.* **98** 115503
[24] Hou Z and Terakura K 2010 Defect states induced by oxygen vacancies in cubic $SrTiO_3$: first-principles calculations *J. Phys. Soc. Japan* **79** 114704
[25] Mitra C, Lin C, Robertson J and Demkov A A 2012 Electronic structure of oxygen vacancies in $SrTiO_3$ and $LaAlO_3$ *Phys. Rev.* B **86** 155105
[26] Carrasco J, Illas F, Lopez N, Kotomin E A, Zhukovskii Y F, Evarestov R A, Mastrikov Y A, Piskunov S and Maier J J 2006 First-principles calculations of the atomic and electronic structure of F centers in the bulk and on the (001) surface of $SrTiO_3$ *Phys. Rev.* B **73** 064106
[27] Lin C, Mitra C and Demkov A A 2012 First-principles calculations of the atomic and electronic structure of F centers in the bulk and on the (001) surface of $SrTiO_3$ *Phys. Rev.* B **86** 161102 (R)
[28] Lin C and Demkov A A 2013 Electron correlation in oxygen vacancy in $SrTiO_3$ *Phys. Rev. Lett.* **111** 217601
[29] Pavlenko N, Kopp T, Tsymbal E Y, Mannhart J and Sawatzky G A 2012 Oxygen vacancies at titanate interfaces: two-dimensional magnetism and orbital reconstruction *Phys. Rev.* B **86** 064431
[30] Kresse G and Hafner J 1993 *Ab initio* molecular dynamics for liquid metals *Phys. Rev.* B **47** 558
[31] Kresse G and Furthmüller J 1996 Efficiency of *ab initio* total energy calculations for metals and semiconductors using a plane-wave basis set *Comput. Mater. Sci.* **6** 15
[32] Blöchl P E 1994 Projector augmented wave method *Phys. Rev.* B **50** 17953
[33] Foyevtsova K, Opahle I, Zhang Y-Z, Jeschke H O and Valentí R 2011 Determination of effective microscopic models for the frustrated antiferromagnets Cs_2CuCl_4 and Cs_2CuBr_4 by density functional methods *Phys. Rev.* B **83** 125126
[34] Perdew J P, Burke K and Ernzerhof M 1996 Generalized gradient approximation made simple *Phys. Rev. Lett.* **77** 3865
[35] Liechtenstein A I, Anisimov V I and Zaanen J 1995 Density functional theory and strong interactions: orbital ordering in Mott–Hubbard insulators *Phys. Rev.* B **52** R5467
[36] Okamoto S, Millis A J and Spaldin N A 2006 Lattice relaxation in oxide heterostructures: $LaTiO_3/SrTiO_3$ superlattices *Phys. Rev. Lett.* **97** 056802
[37] Koepernik K and Eschrig H 1999 Full-potential nonorthogonal local-orbital minimum-basis band-structure scheme *Phys. Rev.* B **59** 1743 http://www.FPLO.de
[38] Bristowe N C, Littlewood P B and Artacho E 2011 Surface defects and conduction in polar oxide heterostructures *Phys. Rev.* B **83** 205405
[39] Zhong Z, Xu P X and Kelly P J 2010 Polarity-induced oxygen vacancies at $LaAlO_3/SrTiO_3$ interfaces *Phys. Rev.* B **82** 165127